**Open Access**

# Segmented Cladding Fiber With a High-Index Ring in Core for Wideband Single-Mode Operation in Any Bending Orientation
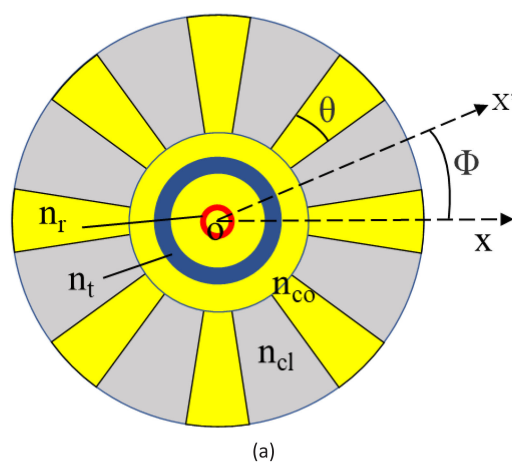
Z. Guo
L. Pei
T. Ning
J. Zheng
J. Li
J. Wang

(a)

# Segmented Cladding Fiber With a High-Index Ring in Core for Wideband Single-Mode Operation in Any Bending Orientation

**Z. Guo, L. Pei, T. Ning, J. Zheng [ID], J. Li, and J. Wang**

Key Lab of All-Optical Network & Advanced Telecommunication Network of EMC, Institute of Lightwave Technology, Beijing Jiaotong University, Beijing 100044, China

**Abstract:** A resonant-ring-assisted large mode area segmented cladding fiber (RR-SCF) with a high-index ring in the core is proposed. Numerical investigations of the effects of the high-index ring on the leakage losses of guiding modes, mode area, and electric field distribution of FM of the proposed fiber show the high-index ring not only increases the ratio of the loss between the fundamental mode (FM) and the higher-order modes (HOMs) but also improves the electric field distribution of the FM to be flat. By taking these advantages of the high-index-ring-assisted core, the effective single-mode (SM) operation is achieved in the proposed fiber bent in any orientation, which makes up the defect of the conventional RR-SCF that the SM output is affected by the bending orientation. Meanwhile, the mode area is enlarged. Furthermore, the effects of the heat load, duty cycle, bending, and operation wavelength on the fiber performance are analyzed. The results show single-mode operation in all bending orientations with a mode area larger than 824 $\mu$m$^2$ can be achieved at a tight bending radius of 15 cm to 16 cm when the operating wavelength ranges from 1.06 $\mu$m to 1.76 $\mu$m. This fiber shows great potential in high-power fiber lasers.

**Index Terms:** Large mode area, high-index ring, single-mode operation, heat load.

## 1. Introduction

Over the last few years, high-power fiber lasers have developed fast due to their advantages such as compact system designs, high output efficiency, good power handling, and better thermal management [1]–[5]. The output power exceeded 10 kW in 2010, just six years after the first demonstration of the 1 kW output laser [6]. However, the further increase of the output power is limited by detrimental phenomena such as optical nonlinear effect, thermal damage, mode instability, and photodarkening [7]–[13]. Among these harmful effects, the nonlinear effect is an urgent problem to be solved.

In order to overcome the difficulty caused by the optical nonlinear effect, several special large mode area (LMA) fibers operating with effective single-mode (SM) are proposed [14]–[15]. These

novel designs include photonic crystal fibers (PCFs) [16], leakage channel fibers (LCFs) [17]–[18], brag fibers (BFs) [19], all-solid photonic bandgap fibers (AS-PBFs) [20], chirally-coupled-core fibers (CCCFs) [21], Gain-guided, index anti-guided fibers (GG+IAGFs) [22], segmented cladding fibers (SCFs) [23], single-trench fibers (STFs) [24], and multi-trench fibers (MTFs) [25]–[26]. Among these elaborate designs with different performances of SM operation and mode areas, SCFs show an attractive prospect due to their all-solid structures and potential to achieve SM operation and large mode area over a wide range of operating wavelengths. SCF was first proposed in 2001 by numerical simulation based on the effective-index method [27]. Its propagation characteristics revealed the potential of SM operation over a wide range of operating wavelengths. Subsequently, SM operation in the SCF made of silver halide materials for the middle infrared was achieved in 2007 [28]. In 2016, the research on the bending performance of the SCF demonstrated the feasibility of SM operation with a large mode area under bending configuration [29]. In 2018, a large mode area SCF with a resonantring (RR-SCF) to enhance the higher-order modes (HOMs) suppression and improve bending performance was proposed [30]. The RR-SCF could provide SM operation in an 18 $\mu$m-radius core at a 15 cm bending radius and showed the possibility to provide SM operation in a larger 25 $\mu$m-radius core. However, as the core size is enlarged to 25 $\mu$m, the SM operation in RR-SCF is affected by the bending orientation of the fiber (this result will be shown in the section of the discussion). It means when the 25 $\mu$m-radius core RR-SCF is utilized as a gain fiber, it has to be coiled in proper bending orientations and without twisting to ensure the HOMs suppression at an acceptable level to keep the beam quality, which would bring difficulties to applications.

   In this paper, a resonant-ring-assisted segmented cladding fiber with a high-index ring in the core is investigated by numerical simulation. The performance improvement of the proposed fiber is demonstrated by the comparison with the performance of the conventional RR-SCF. The fiber performance in practice is verified by taking account into the effect of the heat load. Then the effects of the high-index ring on the performance of the single-mode operation, mode area, and electric field are studied to give a comprehensive understanding of the mechanism of the performance improvement. Besides, the effects of duty cycle, bending radius, and operating wavelength are also analyzed with the consideration of the influence of bending orientation. The proposed fiber can be fabricated by modified chemical vapor deposition (MCVD) process in conjunction with the rod-in-tube method and stack-and-draw technique. The 0.5 $\mu$m thick high-index ring in the core can be fabricated using MCVD technique like the absorbing layer with a designed thickness of 0.446 $\mu$m in Ref. [31]. The performance of single-mode operation with a large mode area over a range of wavelengths makes the fiber a good candidate for fiber lasers.

## 2. Fiber Design and Analysis Methodology

We propose a resonant-ring-assisted segmented cladding fiber with a high-index ring in the core (HIR-RR-SCF), as shown in Fig. 1. In Fig. 1(a), the yellow region represents a high refractive index of $n_{co}$. The gray region represents a low refractive index of $n_{cl} = n_{co} - \Delta n_1$. The blue ring is a low-index trench with a refractive index of $n_t = n_{co} - \Delta n_2$. The red ring inside the core stands for a high index of $n_r = n_{co} + \Delta n$. $\theta$ is the fan angle of high-index segments and is described by duty cycle $\gamma$. The duty cycle $\gamma$ is defined as $\gamma = 1 - \theta/(360/N)$, where $N$ is the number of the segmentation, here is 8. $\Phi$ is the angle between the bending orientation x' and the reference orientation x. The refractive index profiles of the fiber along the x-direction and x'-direction are shown in Fig. 1(b). In Fig. 1(b), t is the thickness of the high-index ring in the core, $t_r$ is the thickness of the index trench, d is the thickness of the resonant ring, $r_r$ is the outer radius of the high-index ring. Furthermore, a and b are the core radius and cladding radius, respectively. The definitions of these parameters and the parameters in later simulations are listed in Table 1 to give a clear view.

   In this research, the commercial software COMSOL multi-physics based on the finite element method (FEM) was used for numerical simulation. An isotropic 20 $\mu$m thick circular perfectly matched layer (PML) is set outside the fiber cladding to truncate the computing domain. The fiber cross-section was discretized into 5314 finite element meshes with a maximum size of
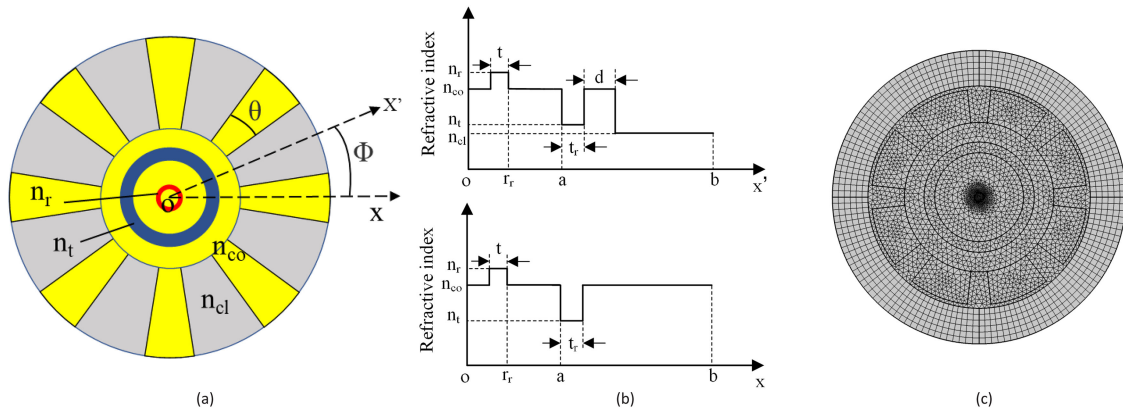
Fig. 1. (a) Cross-section of the proposed resonantring (the yellow ring around the blue ring) assisted segmented cladding fiber with a high-index ring (red) in the core. $n_{co}$ is the refractive index of the core, resonant ring, and the high-index segments. $n_r$, $n_t$, and $n_{cl}$ are the refractive index of the high-index ring, index trench, and low-index segments, respectively. $\Theta$ is the fan angle of the high-index segments and $\Phi$ is the bending orientation angle. (b) Refractive index profiles of the proposed fiber along the x-axis and x'-axis. a, b, and $r_r$ are the radii of the core, cladding, outer radius of the high-index ring, respectively. t, $t_r$, and d are the thicknesses of the high-index ring, index trench, and resonantring, respectively. (c) Discretization of the fiber cross-section into finite elements.

TABLE 1
Definitions of Fiber Parameters and the Parameters of the RR-SCF and HIR-RR-SCF

| Definitions | RR-SCF | HIR-RR-SCF |
|---|---|---|
| Index of core and high-index cladding $n_{co}$ | 1.451 | 1.451 |
| Index of low-index cladding $n_{cl}$ | 1.445 | 1.445 |
| Index of high-index ring $n_r$ | | 1.452 |
| Index of index trench $n_t$ | 1.445 | 1.449 |
| Core radius a (μm) | 25 | 25 |
| Cladding radius b (μm) | 62.5 | 62.5 |
| Outer radius of high-index ring $r_r$ (μm) | | 3 |
| Thickness of index trench $t_r$ (μm) | 3 | 6 |
| Thickness of high-index ring t (μm) | | 0.5 |
| Thickness of the resonant ring d (μm) | 11 | 11 |
| Number of segmentation $N$ | 8 | 8 |
| Duty cycle γ | 0.7 | 0.72 |
| Bending orientation angle Φ | 0 | 0 |
| Bending radius $R_b$ (cm) | 15 | 15 |
| Wavelength λ (μm) | 1.06 | 1.06 |

3.3 $\mu$m as shown in Fig. 1(c). The refractive index of the PML is the same as those of the high-index segmented cladding and the mapped meshes were applied to discretize the PML [24]. In order to investigate the bending performance of the proposed fiber, the equivalent index transformation for bending with additional stress perturbations is applied. The formula is expressed as [32]:

$$n_{\text{bent}} = n_{\text{straight}} \left( 1 + \frac{x \cdot \cos \phi + y \cdot \sin \phi}{\rho \cdot R_b} \right) \tag{1}$$

where $n_{\text{bent}}$ and $n_{\text{straight}}$ are the refractive indexes of the bent fiber and straight fiber respectively. In addition, x and y are the coordinates in Cartesian coordinate system, in which the coordinate origin o is the center of the core (as shown in Fig. 1(a)). $\Phi$ is the bending orientation angle to the reference orientation. $\rho$ is the elasto-optical coefficient (here fixed to 1.25) which is included to take account of the stress factor [33]. $R_b$ is the bending radius of the fiber.

The performance of the SM operation is evaluated by the leakage losses of the FM and HOMs. Previous studies have concluded that the highest leakage loss of the FMs with both two polarizations which is lower than 0.1 dB/m and the lowest leakage loss of the HOMs with all possible polarizations and orientations which is greater than 1 dB/m is the baseline for SM operation [34]. The leakage losses of the guiding modes (dB/m) which mainly include the macro bending mode loss and intrinsic mode loss of the fiber are calculated by [35]:

$$Loss = \frac{40\pi}{\lambda \ln 10} \, \text{Im} \, (n_{eff}) \tag{2}$$

where $n_{eff}$ is the effective refractive index of the core mode and $\lambda$ is the operating wavelength. It should be noted that the FM loss in later discussion refers to the highest loss of the FMs with two polarizations.

In addition, the higher-order mode extinction ratio (HOMER) of the lowest HOM loss to the highest FM loss is also used to evaluate SM operation [36]–[37]. Corresponding to the limit of the highest loss of the FM and the lowest loss of HOMs, a HOMER greater than 10 is the baseline for SM operation.

The effective area of FM (mode area) $A_{eff}$ is expressed as [30]:

$$A_{eff} = \frac{\left( \iint_s |E(x, y)|^2 dxdy \right)^2}{\iint_s |E(x, y)|^4 dxdy} \tag{3}$$

where $E(x, y)$ is the transverse component of the electric field in the fiber and integral region S is the cross-section of the fiber.

Considering the actual performance of the fiber in applications, the effect of the thermal load needs to be investigated. The refractive index of the bent fiber under heat load is expressed as in Eq. (4), shown at bottom of the next page [9], [38]–[39].

Where $c$ is the radius of the fiber coating, $\beta$ is the thermal optical coefficient that describes the index change per Kelvin, $k_{si}$ and $k_c$ are the thermal conductivity for the silica and coating material, $h$ is the convective coefficient between the coat and air. In addition, $q$ is the heat load density which can be expressed as [9]:

$$q(z) = \frac{Q(z)}{\pi a^2} \tag{5}$$

Where $Q(z)$ is the heat load. The parameters for calculating the performance of the fiber under heat load are listed in Table 2.

TABLE 2

Parameters for Calculating the Performance of the Proposed Fiber Under Heat Load

| Parameter | Value | Parameter | Value |
|---|---|---|---|
| c | 125 μm | h | 80 W/(m$^2$×K) [39] |
| $k_{si}$ | 1.38 W/(m×K) [9] | β | 3×10$^{-5}$/K [9] |
| $k_c$ | 0.2 W/(m×K) [9] | | |

## 3. Results and Discussions

### 3.1. Performance of the Proposed Fiber

To demonstrate the importance of the high-index ring in the core, the performance of the proposed fiber is firstly compared with that of the reported resonant-ring-assisted segmented cladding fiber [30]. The effects of bending orientation on the leakage losses of the guiding modes and the mode area of the reported RR-SCF and our proposed HIR-RR-SCF are shown in Fig. 2. The parameters of the RR-SCF are the same as those in literature [30] and are listed in Table 1 together with the parameters of our proposed HIR-RR-SCF. As these two fibers are not circularly symmetric, the performance of the fibers bent in different orientations from 0° to 22.5° needs to be considered. In Fig. 2, the first three lowest HOM losses are shown. From Fig. 2(a), although the leakage loss of LP$_{01}$ mode (FM) of the RR-SCF is kept lower than 0.1 dB/m when the bending orientation varies, the lowest loss of the HOMs isn't higher than 1 dB/m when the bending orientation angle $\Phi \leq 4.5°$, which can't meet the requirement for effective single-mode operation. This sensitivity to bending orientation means when it is applied as a gain medium in a fiber laser system, the coiled RR-SCF has to be properly fixed to avoid the degradation of HOMs suppression. From Fig. 2(b), the lowest HOM loss is always higher than 2.48 dB/m and the FM loss is lower than 0.1 dB/m no matter which orientation the proposed fiber is bent in. Therefore, SM operation can be maintained in the proposed fiber with all the bending orientations. This improvement of SM operation is attributed to the improved HOMER (this result will be analyzed in the discussion about Fig. 4). Furthermore, the mode area of the proposed fiber is 824 $\mu$m$^2$, which is about 34 $\mu$m$^2$ larger than that of the RR-SCF. This mode area scaling indicates the feasibility of the approach of introducing a high-index structure in the core to improve the electric field distribution to be more even.

$n_T \ (q, r)$

$$
= \begin{cases}
\left(n_{co} + \frac{qa^2\beta}{4k_{si}}\left[1 + \frac{2k_{si}}{hc} + 2\ln\left(\frac{b}{a}\right) + 2\frac{k_{si}}{k_c}\ln\left(\frac{c}{b}\right) - \left(\frac{r}{a}\right)^2\right]\right) \\
\times \left(1 + \frac{x\cos\Phi + y\sin\Phi}{\rho \cdot R_b}\right), \\
\hfill 0 \leq r \leq r_r - t,\ r_r \leq r \leq a \\
\left(n_r + \frac{qa^2\beta}{4k_{si}}\left[1 + \frac{2k_{si}}{hc} + 2\ln\left(\frac{b}{a}\right) + 2\frac{k_{si}}{k_c}\ln\left(\frac{c}{b}\right) - \left(\frac{r}{a}\right)^2\right]\right) \times \left(1 + \frac{x\cos\Phi + y\sin\Phi}{\rho \cdot R_b}\right),\ r_r - t \leq r \leq r_r \\
\left(n_{tr} + \frac{qa^2\beta}{2k_{si}}\left[\frac{k_{si}}{hc} + \ln\left(\frac{b}{r}\right) + \frac{k_{si}}{k_c}\ln\left(\frac{c}{b}\right)\right]\right) \times \left(1 + \frac{x\cos\Phi + y\sin\Phi}{\rho \cdot R_b}\right),\ a \leq r \leq a + t_r \\
\text{for high} - \text{index ring and cladding}: \left(n_{co} + \frac{qa^2\beta}{2k_{si}}\left[\frac{k_{si}}{hc} + \ln\left(\frac{b}{r}\right) + \frac{k_{si}}{k_c}\ln\left(\frac{c}{b}\right)\right]\right) \times \left(1 + \frac{x\cos\Phi + y\sin\Phi}{\rho \cdot R_b}\right), \\
\hfill a + t_r \leq r \leq b \\
\text{for low} - \text{index segmented cladding}: \left(n_{cl} + \frac{qa^2\beta}{2k_{si}}\left[\frac{k_{si}}{hc} + \ln\left(\frac{b}{r}\right) + \frac{k_{si}}{k_c}\ln\left(\frac{c}{b}\right)\right]\right) \times \left(1 + \frac{x\cos\Phi + y\sin\Phi}{\rho \cdot R_b}\right), \\
\hfill a + t_r \leq r \leq b
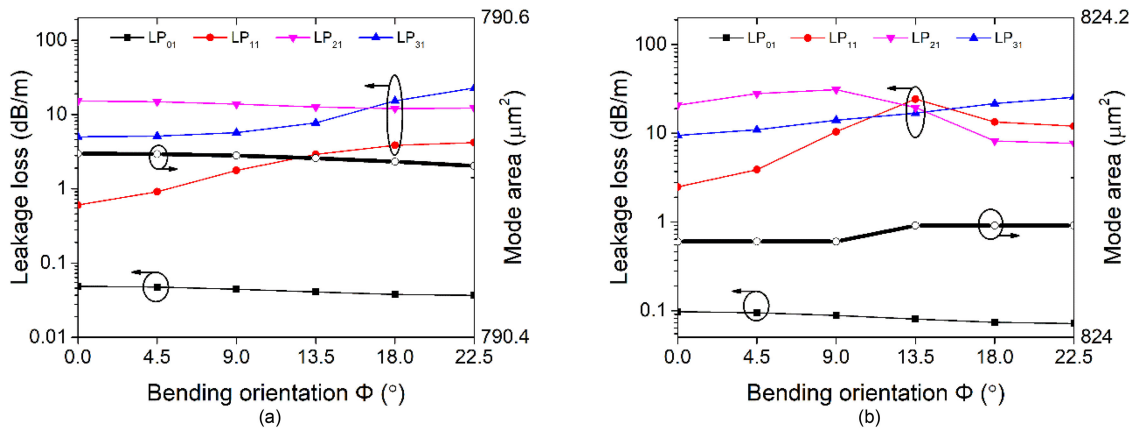\end{cases}
$$

$$(4)$$

Fig. 2. Variations of leakage losses and mode area of (a) the RR-SCF and (b) the HIR-RR-SCF with the bending orientation when the operating wavelength is 1.06 $\mu$m and the bending radius is 15 cm. The parameters of these two fibers are listed in Table 1 except the bending orientations are variables.
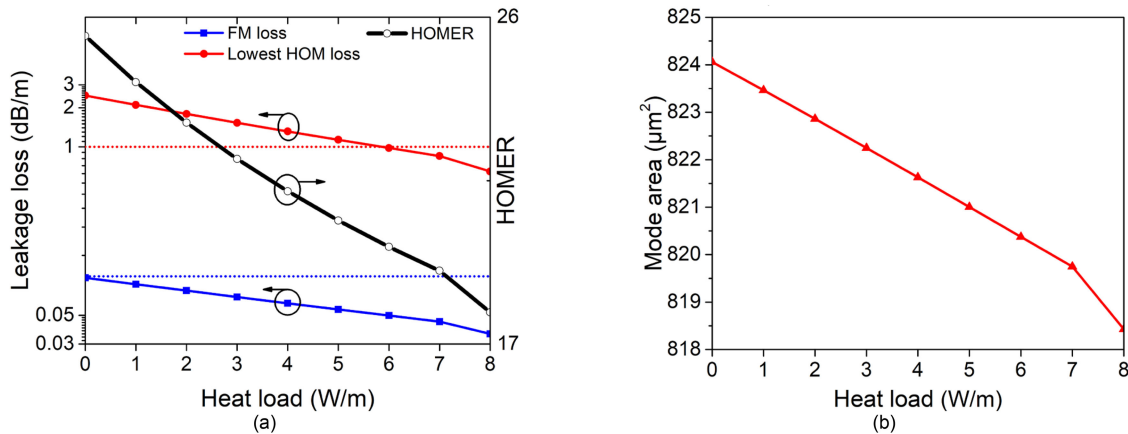


Fig. 3. (a) The FM loss, lowest HOM loss, and HOMER and (b) mode area of the proposed fiber under heat load (The parameters are listed in Table 1 and Table 2).

The performance of the fiber under heat load calculated by the formula (4) and (5) is shown in Fig. 3. From Fig. 3(a), both the FM loss and the lowest HOM loss decrease monotonically as the heat load rises. The lowest HOM loss is reduced to 1 dB/m when the head load reaches 6 W/m, which means the SM operation is no longer maintained. Furthermore, the HOMER also decreases monotonically with the increase of the heat load, which means it becomes more and more difficult to strip off the HOMs to realize SM operation. Fig. 3(b) shows the mode area also deteriorates with the increase of heat load. All the results in Fig. 3 demonstrate SM operation with a mode area of larger than 821 $\mu$m$^2$ can be achieved when the heat load is controlled within 5W/m.

## 3.2. Effects of the High-Index Ring Parameters

Since the high-index ring in the core brings the improvement of SM operation and enlargement of mode area, the effect of changes of its parameters on the performance of the optical fiber needs to be investigated in detail. It should be noted the effect of the heat load is no longer considered in this paper because we need to first figure out the performance of the optical fiber under bending configuration. Fig. 4 shows the effect of the thickness of the high-index ring on the performance of
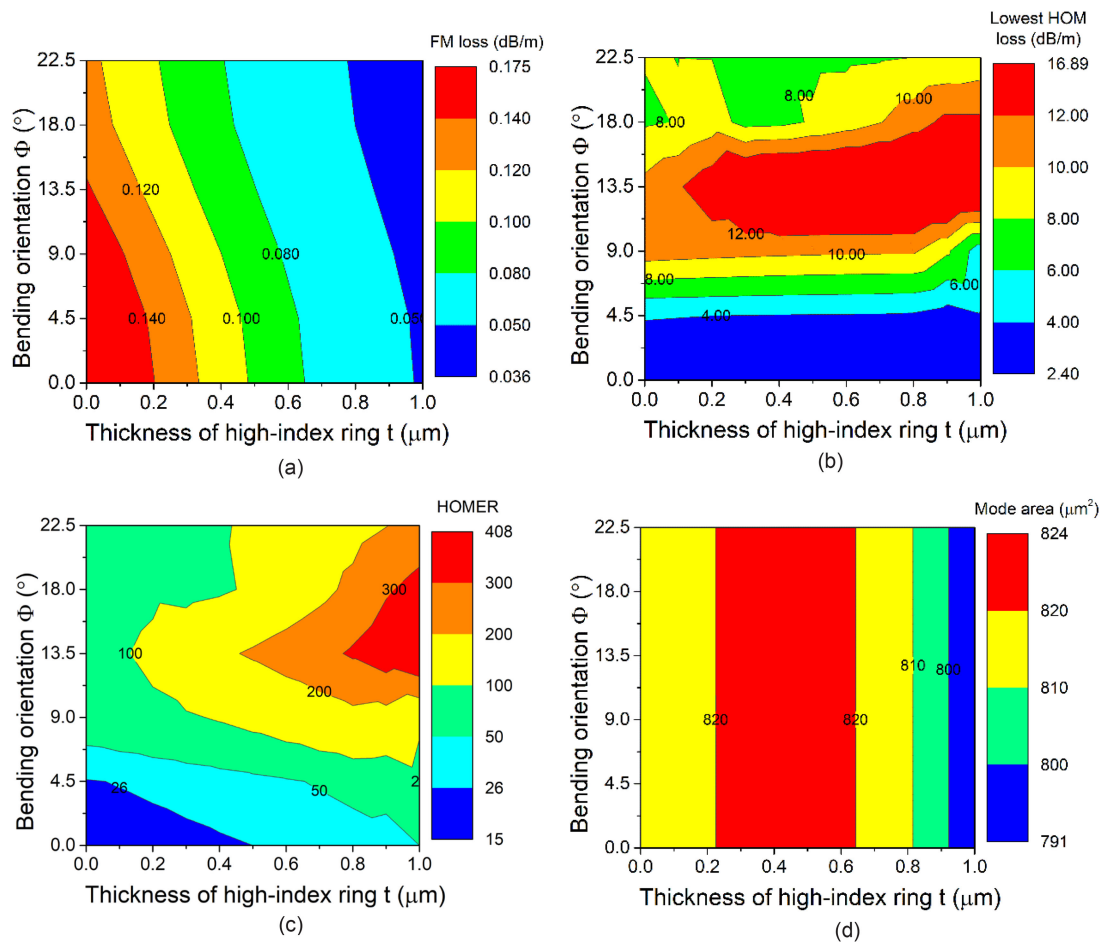
Fig. 4. Effects of the thickness of the high-index ring on (a) the FM loss, (b) the lowest HOM loss, (c) the HOMER, and (d) the mode area of the proposed fiber when the bending orientation changes (The parameters are listed in Table 1 except t and $\Phi$ are variables).

the fiber. The influence of the bending orientation is still considered. The parameters are the same as those listed in Table 1 except the thickness of high-index ring t is set as a variable. In addition, t = 0 is equivalent to the absence of the high-index ring which refers to the RR-SCF. From Fig. 4(a), the FM loss decreases monotonically from higher than 0.14 dB/m to lower than 0.05 dB/m as the high-index ring becomes thicker. It means the capability of the core to confine light is enhanced when the high-index ring is introduced (t = 0.1 $\mu$m) and positively related to t when t is appropriate. When t $\geq$0.5 $\mu$m, the FM loss in the fiber bent in all orientations is lower than 0.1 dB/m to meet the requirement for SM operation. It can also be found the FM loss decreases monotonically with the increase of the bending orientation angle. This variation is attributed to the enhancement of the cladding effect with the increase of the cladding thickness when bending orientation increases from 0° to 22.5°. Fig. 4(b) shows the lowest HOM loss changes very slowly with the increase of the thickness of the high-index ring but increases obviously from lower than 4 dB/m to higher than 12 dB/m when $\Phi$ increases from 0° to 13.5° and then decreases with the further increase of $\Phi$. It's clear to see the lower sensitivity of the HOM loss to the thickness of the high-index ring is due to the fact that the location of the high-index ring doesn't well overlap with the region where much power fraction of HOMs located according to the general characteristics of the electric distributions of the guiding modes in optical fiber. It's also clear that the sensitivity of HOMs loss to bending orientation

is attributed to the power distribution of the HOMs which is closer to the cladding and easily affected by the intrinsic refractive index change of the segmented cladding in the circumferential direction. Although the HOMs are inevitably sensitive to bending orientation, the lowest HOM loss of 2.4 dB/m when $\Phi = 0°$ which corresponding to the worst condition of HOMs suppression ensures the HOMs suppression meets the requirement for SM operation. Fig. 4(c) shows the HOMER increases from smaller than 26 to greater than 300 when the high-index ring is introduced and becomes thicker. Furthermore, the HOMER is sensitive to the bending orientation. It increases sharply when the bending orientation increases from 0° to 13.5° and then drops with the further increase of the bending orientation. This dependence of the HOMER on bending orientation agrees well with the variations of the FM loss and the lowest HOM loss. From Fig. 4(d), the mode area is independent of the bending orientation. It increases firstly from 811 $\mu m^2$ to 824 $\mu m^2$ when the thickness of the high-index ring increases from 0 to 0.5 $\mu m$ and then decreases to smaller than 800 $\mu m^2$ with the further increase of the thickness of the high-index ring. This trend indicates a high-index ring with an appropriate thickness is beneficial to the mode area but a too thick high-index ring would lead to the power focusing in the core which reduces the mode area. From all the results in Fig. 4, SM operation in the fiber bent in any orientation can be achieved when t≥0.5 $\mu m$. Furthermore, the mode area can be enlarged to 824 $\mu m^2$ when t = 0.5 $\mu m$. This improvement of the fiber performance shows the feasibility and potential of SM operation and mode area enlargement of SCF by adding a high-index ring with suitable thickness.

In order to give an understanding of the effect of the high-index ring on the mode area, the electric field distribution of FM in the fiber was investigated. Fig. 5 shows the normalized electric field distributions with contours of FM in the HIR-RR-SCFs with different thickness high-index rings in the core. The effect of bending orientation on the electric field distribution is also considered by investigating electric field distribution in the fiber with bending orientations vary by 9°. The parameters in Fig. 5 are the same as those in Fig. 4. In Fig. 5, the horizontal and vertical wireframes are added to ensure a set of nodes of finite element mesh would be created along the x-axis and y-axis in order to see whether the maximum electric field intensity is located on the bending orientation (i.e. the x-axis) and the symmetry of the electric field with respect to the bending orientation. The bending orientations of the horizontal-right in the second and third rows in Fig. 5(a) are equivalent to the bending orientations of 9° and 18° in Fig. 1(a) since the geometries in the second and third rows are obtained from the clockwise rotations of the geometry in Fig. 1(a). This equivalence is for the sake of the convenience of cutting a line of data collection from the whole set of solutions of the numerical model. To give a clear view of electric field distributions in the core with the submicron thick high-index rings, the parts of the cladding of the proposed fiber are no longer shown in Fig. 5(a). From the first row of Fig. 5(a), the bend-induced mode distortion in the fiber with a bending orientation of 0° is improved as the high-index ring is introduced and thickened to 0.5 $\mu m$. It also shows the maximum electric field intensity is located closer to the high-index ring when the high-index ring becomes thicker. When t = 0.8 $\mu m$ and t = 1 $\mu m$ the maximum electric field intensity is in the region of the high-index ring. This variation of the electric field indicates the power focusing in the high-index ring becomes stronger when the high-index ring is thickened which would be harmful to inhibition of non-linear effects since a new power peak is produced. From the electric distributions in the second and third rows of Fig. 5(a), the variations of the electric field with the thickness of the high-index ring are the same as that in the fiber bend in the orientation of 0°. The effect of the high-index ring in the electric field is nearly independent of the bending orientation of the fiber. The left figures in Fig. 5(b) show the normalized electric field distribution along the x-axis becomes fatter when the high-index ring is added. The profile is further flattened when the thickness of the high-index ring increases from 0.2 $\mu m$ to 0.5$\mu m$. However, when the high-index ring becomes thicker to 0.8 $\mu m$ and 1 $\mu m$, the electric field intensity profile is degraded more and more seriously since more power is focused in the high-index region. The right figures in Fig .5(b) show the electric field distributions along the y-axis. It should be noted the electric field intensity data in Fig. 5(b) is cut from a line parallel to the y-axis and passing through the point of the maximum electric field in the solution set. From Fig. 5(b), when t = 0.2 $\mu m$ and t = 0.5 $\mu m$ the electric field distribution along the y-axis is almost the same as that of the RR-SCF (t = 0) since
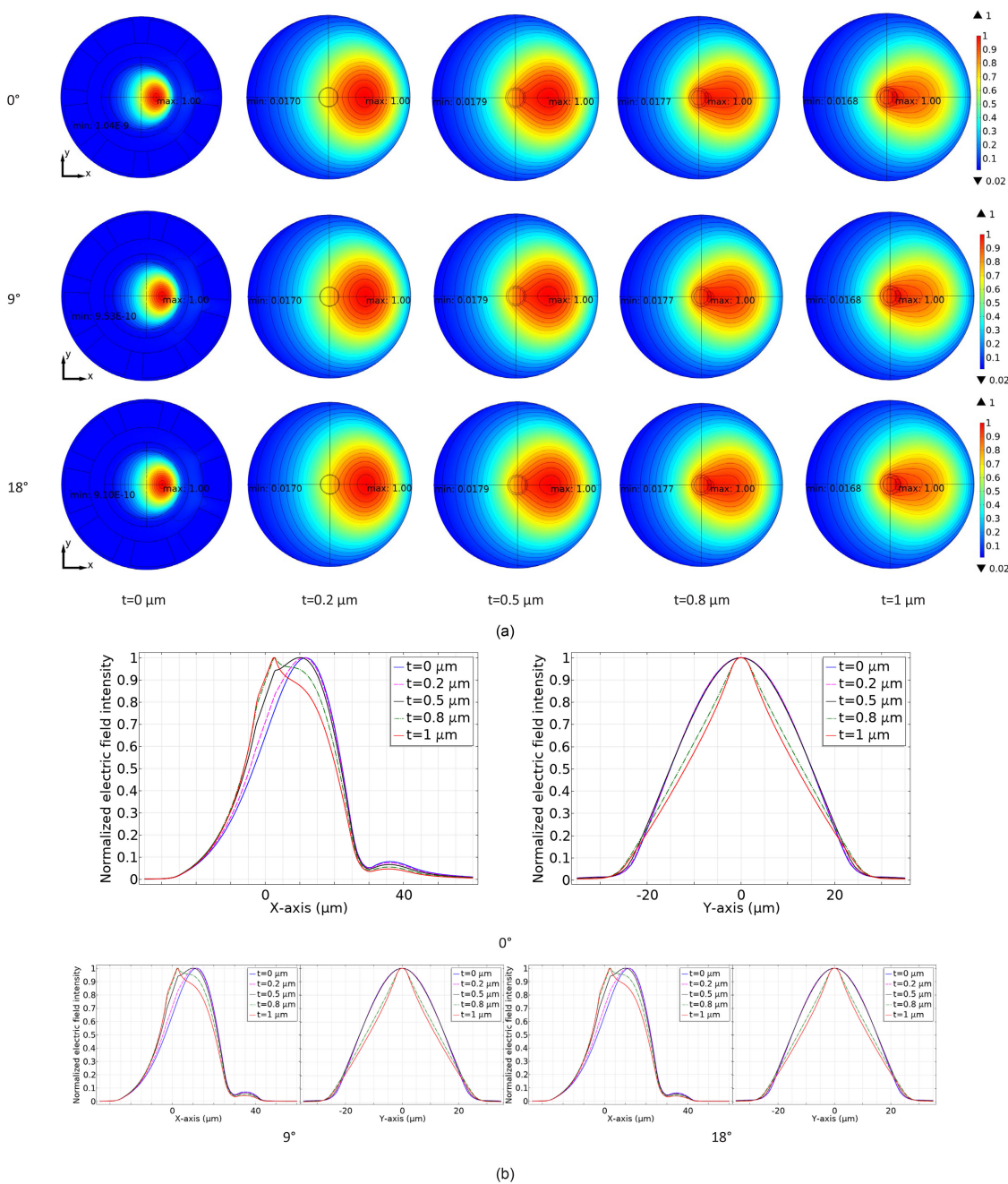
Fig. 5. (a) Electric field distributions of the FM and (b) electric field profiles along the x-axis and y-axis in the proposed fibers with different thickness high-index rings in the core when the bending orientation angle is 0°, 9°, and 18°, respectively (The parameters are the same as those in Fig. 4).

the effect of the thin high-index ring is so weak. However, as the high-index ring becomes thicker to 0.8 $\mu$m and 1 $\mu$m, the top of the electric field intensity profile becomes sharp as more power is confined to the high-index region. Furthermore, the comparison of the electric field profiles in the fiber bent in different orientations shows again the bending orientation has almost no effect on the electric field distribution in the core. Fig. 5(a) and (b) explain well why the mode area enlarges
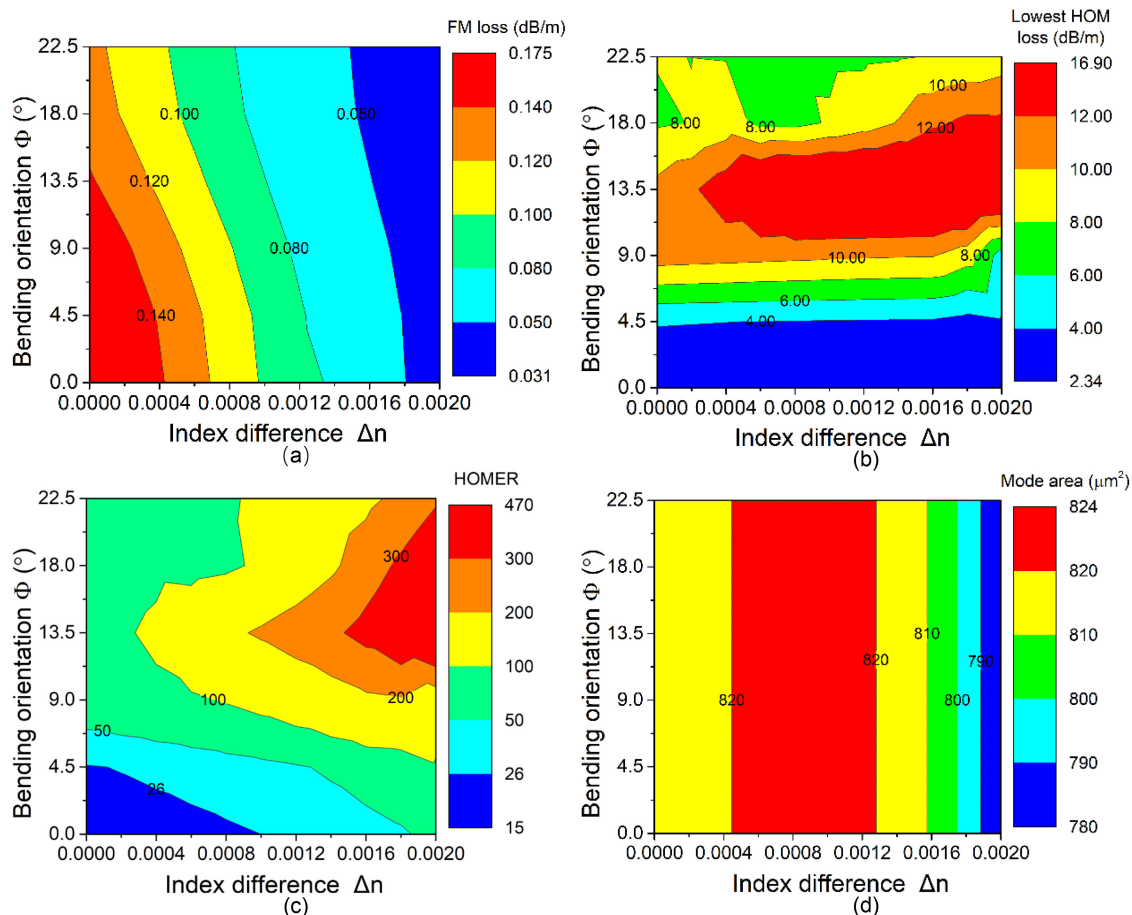
Fig. 6. Effects of the index difference $\Delta n$ on (a) the FM loss, (b) the lowest HOM loss, (c) the HOMER, and (d) the mode area of the proposed when the bending orientation changes (The parameters are listed in Table 1 except $\Delta n$ and $\Phi$ are variables).

first and then decreases when the high-index ring becomes thicker as shown in Fig. 4(d). It can be concluded from Fig. 5, the electric distribution can be improved flattened to enlarge the mode area by the high-index ring with an appropriate thickness. In addition, the effect of the high-index ring on the electric field distribution is almost independent of the bending orientation.

The effects of the index difference between the high-index ring and the core $\Delta n$ on the performance of the fiber are shown in Fig. 6. The parameters are the same as those in Table 1 except $\Delta n$ is a variable. It's worth noting $\Delta n = 0$ is equivalent to the absence of the high-index ring. From Fig. 6(a), the FM loss decreases monotonically from higher than 0.14 dB/m to lower than 0.05 dB/m with the increase of $\Delta n$ and $\Phi$. This is attributed to the enhanced capability of the core to confine light when $\Delta n$ is increased. Furthermore, when $\Delta n \geq 0.001$, the FM loss is always lower than 0.1 dB/m no matter which orientation the fiber is bent in. Fig. 6(b) shows the lowest HOM loss is slightly affected by $\Delta n$ but sensitive to the bending orientation. However, the lowest HOM loss is always higher than 2.34 dB/m to ensure the HOMs suppression at an acceptable level. From Fig. 6(c), the HOMER increases from 15 to 470 with the increase of $\Delta n$ when $\Phi$ is appropriate. The dependence of the HOMER on $\Delta n$ and $\Phi$ agrees well with the variations of the FM loss and lowest HOM loss. Fig. 6(d) shows the mode area is independent of the bending orientation. It increases from 811 $\mu m^2$ to 824 $\mu m^2$ first and then decreases to smaller than 790 $\mu m^2$ with the continuous increase of $\Delta n$. This result indicates in order to enlarge the mode area, $\Delta n$ should be controlled in a proper
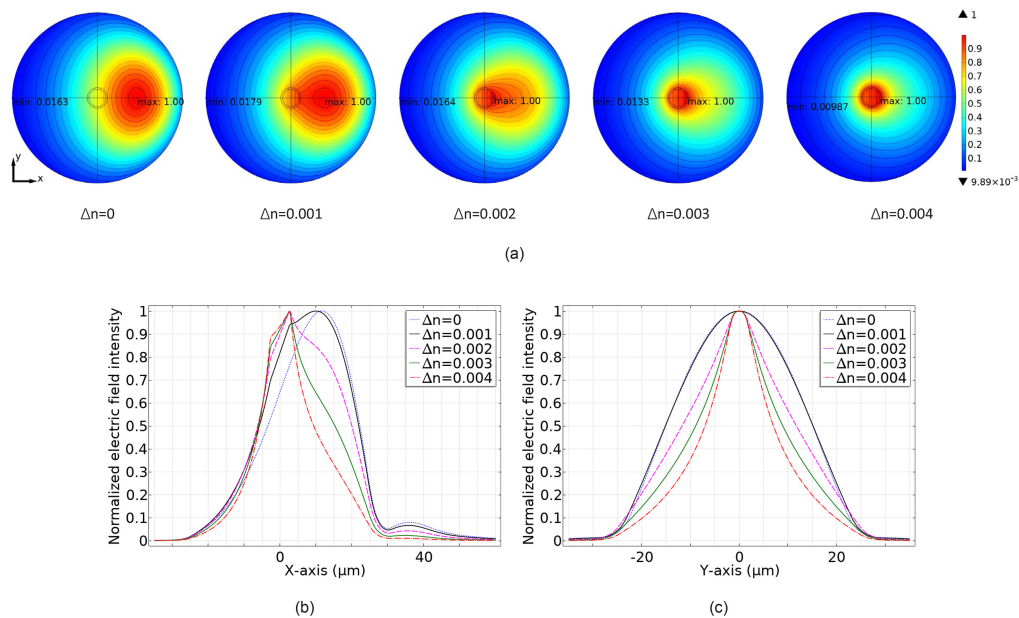
Fig. 7. (a) Electric field distributions of FM and (b) electric field profiles along the x-axis and (c) y-axis in the proposed fibers with different index differences between the high-index ring and the core (The parameters are the same as those in Fig. 6).

range. From all the results in Fig. 6, to achieve SM operation and LMA, $0.001 \leq \Delta n \leq 0.0013$ is appropriate. Moreover, it's interesting and amazing to see the results in Fig. 6 are highly similar to the results showed in Fig. 4. By the comparison between Fig. 4 and Fig. 6, to a certain extent, the effects of increasing $\Delta n_1$ on the loss of guiding modes and mode area are similar to the effects of increasing the thickness of the high-index ring. This conclusion indicates the SM operation with LMA can be achieved either by adjusting the thickness of the high-index ring or by controlling the index difference between the high-index ring and the core.

The effect of $\Delta n$ on the electric field distribution of FM in the fiber is shown in Fig. 7. The parameters are the same as those in Fig. 6. Considering the fabrication feasibility of the minimum index difference in silica glass, the dependence of the electric field on the index difference is investigated when $\Delta n$ increases with a step of 0.001. Furthermore, the effect of bending orientation on the electric field of FM is no longer displayed in detail since it can almost be ignored as mentioned in the previous discussion of the effect of thickness of high-index ring on the electric field. From Fig. 7(a), the mode distortion is improved when the high-index ring is introduced in the core ($\Delta n = 0.001$). However, as $\Delta n$ increases continuously from 0.001 to 0.004, the electric power is more and more focused in the high-index ring region, which would lead to a new higher power peak and a big discount of the mode area. From Fig. 7(b), the electric field distribution along the x-axis in the core when $\Delta n = 0.001$ is fatter than that in the core without a high-index ring ($\Delta n = 0$). However, when $\Delta n$ increases from 0.001 to 0.004, the electric field intensity profile becomes thinner obviously since most of the power is distributed in the high-index ring region. From Fig. 7(c), the electric field distribution along the y-axis which includes the electric field peak almost keeps the same when the high-index ring is introduced ($\Delta n = 0.001$). However, the profile becomes thinner when $\Delta n$ increases from 0.001 to 0.004, which indicates the mode area is sharply reduced since the electric power is excessively concentrated in the high-index ring. In summary, from all the results in Fig. 7, a proper index difference between the high-index ring and the core is beneficial to a flat-top electric field distribution in the proposed fiber.
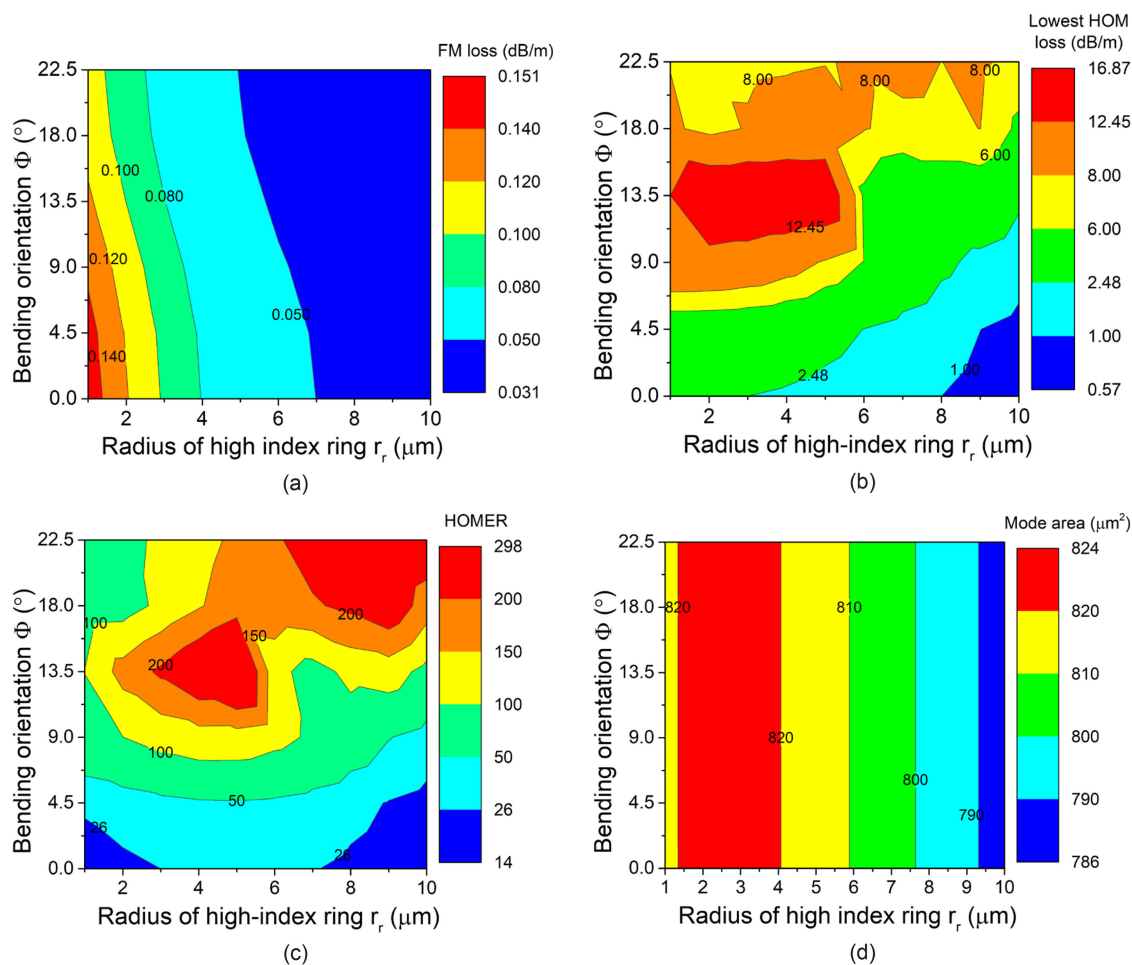
Fig. 8. Effects of the radius of the high-index ring on (a) the FM loss, (b) the lowest HOM loss, (c) the HOMER, and (d) the mode area of the proposed fiber when the bending orientation changes (The parameters are listed in Table 1 except rr and Φ are variables).

The effects of the radius of the high-index ring on the performance of the fiber are shown in Fig. 8. The parameters are the same as those in Table 1 except the outer radius of the high-index ring $r_r$ is a variable. From Fig. 8(a), the FM loss decreases monotonically from higher than 0.14 dB/m to lower than 0.05 dB/m when $r_r$ increases from 1 $\mu$m to 10 $\mu$m. When $r_r \geq 3$ $\mu$m the FM loss is always lower than 0.1 dB/m no matter which orientation the fiber is bent in. From Fig. 8(b), the lowest HOM loss decreases with the increase of $r_r$. However, the lowest HOM loss is always higher than 1 dB/m in the fiber bent in any orientation when $r_r \leq 8$ $\mu$m. Especially when $r_r \leq 3$ $\mu$m, a lowest HOM loss not lower than 2.48 dB/m can be achieved in the fiber bent in any orientation. From Fig. 8(c), the HOMER is always larger than 26 when 3 $\mu$m$\leq r_r \leq 7$ $\mu$m even the bending orientation varies. From Fig. 8(d), the mode area can be enlarged to 824 $\mu$m² when $r_r$ is appropriate. From all the results in Fig. 8, SM operation can be achieved when 3 $\mu$m$\leq r_r \leq 8$ $\mu$m. When $r_r = 3$ the mode area reaches the largest 824 $\mu$m².

The effect of the radius of the high-index ring on the normalized electric field of FM is shown in Fig. 9. The parameters are the same as those in Fig. 8. the effect of bending orientation on the electric field is no longer displayed, either. From Fig. 9(a), the mode distortion is improved when $r_r$ increases from 1 $\mu$m to 3 $\mu$m. When $r_r$ increases continuously to larger than 3 $\mu$m, the maximum electric field occurs in the high-index ring region. From Fig. 9(b), the electric field distribution along
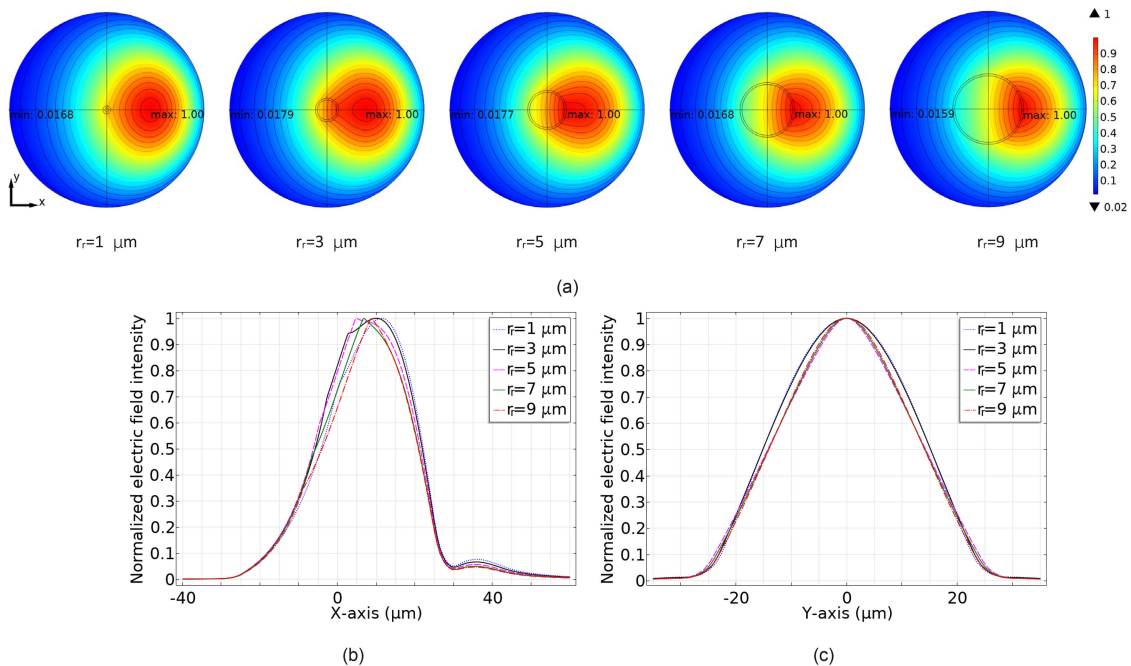
Fig. 9. (a) Electric field distributions of FM and (b) electric field profiles along the x-axis and (c) y-axis in the proposed fibers with high-index rings of different radii (The parameters are the same as those in Fig. 8).

the x-axis is fatter when $r_r = 3 \ \mu m$ than when $r_r = 1 \ \mu m$. However, as the $r_r$ further increases, the top of the electric field distribution becomes sharp, which indicates degradation of the power distribution and mode area. Fig. 9(c) shows when $r_r$ increases from 1 $\mu m$ to 3 $\mu m$, the electric field distribution along the y-axis profile is almost unchanged. However, the electric field intensity profile becomes thinner when $r_r$ increases to 5 $\mu m$ and larger. Fig. 9(b) and Fig. 9(c) explain well why the mode area increases first and then decreases with the increase of $r_r$ as shown in Fig. 8(d). All the results in Fig. 9 indicate flat-top power distribution of FM can be achieved for a large mode area if the high-index ring is designed with a proper radius.

From the above studies of the high-index ring, the high-index structure in the core could generally enhance the capability of the core to confine light, but its effects on the FM and HOMs are different. By taking advantage of this difference and adjusting the effect of the cladding, the HOMs suppression can be enhanced to achieve single-mode operation. In addition, the electric field can be flattened without generating new power peaks by the well-designed high-index ring. The mode area can thus be enlarged as a result of the more uniform power distribution.

### 3.3. Effects of Other Parameters

As the effects of the index trench of the cladding and the resonantring are similar to those of the RR-SCF and have been analyzed in detail in Ref. [30], they are no longer discussed in this paper. Other parameters such as the duty cycle of the cladding, bending radius, and the operating wavelength are investigated to give a comprehensive knowledge of the fiber.

The effects of the duty cycle of the cladding on the FM loss, the lowest HOM loss, the HOMER, and the mode area are shown in Fig. 10. From Fig. 10(a), the FM loss decreases monotonically from higher than 1 dB/m to lower than 0.05 dB/m when $\gamma$ increases from 0.67 to 0.75. When $\gamma \geq 0.72$, the FM loss is always lower than 0.1 dB/m no matter which orientation the fiber is bent in. From Fig. 10(b), when $\gamma \leq 0.73$ the lowest HOM loss is always higher than 1 dB/m. From Fig. 10(c),
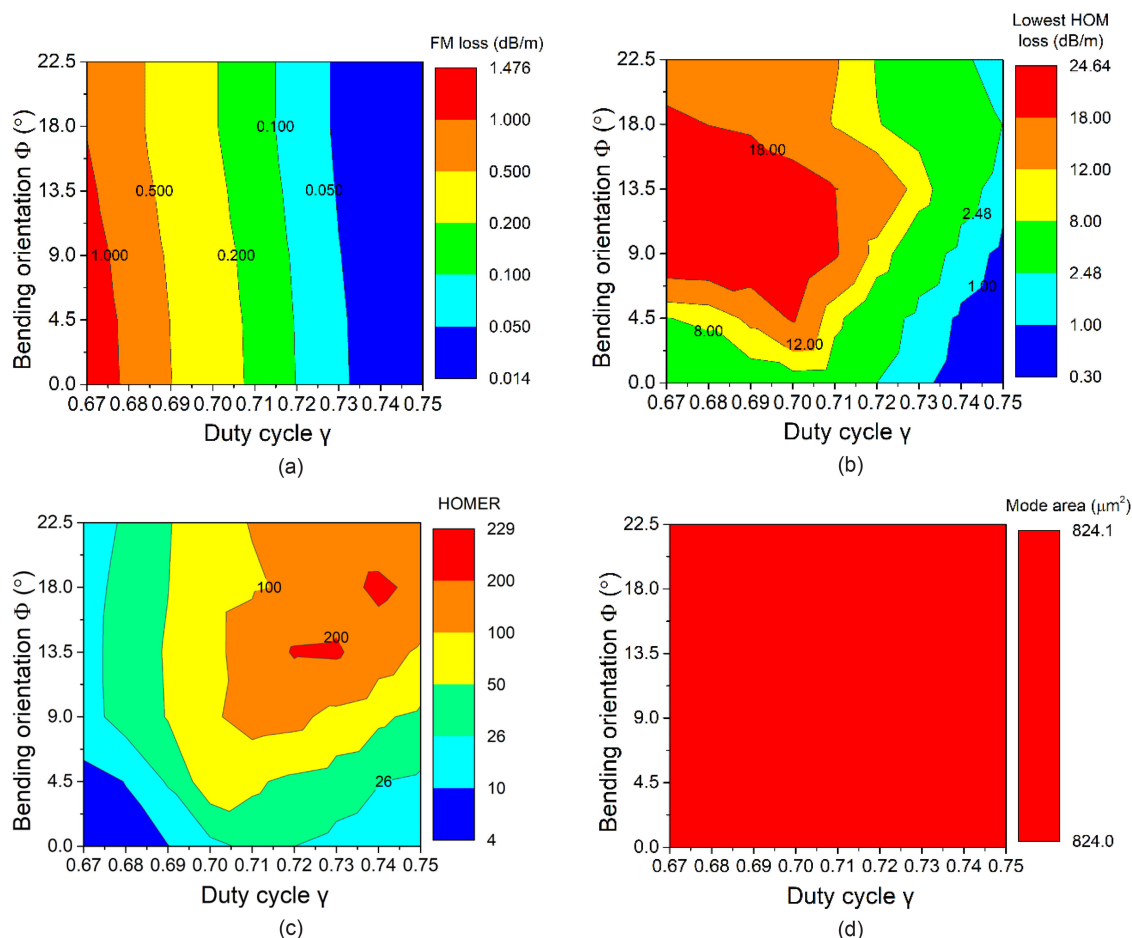
Fig. 10. Effects of the duty cycle on (a) the FM loss, (b) the lowest HOM loss, (c) the HOMER, and (d) the mode area of the proposed fiber when the bending orientation changes (The parameters are listed in Table 1 except $\gamma$ and $\Phi$ are variables).

the HOMER is always greater than 10 when $\gamma \geq 0.69$. When $0.705 \leq \gamma \leq 0.72$, the HOMER $\geq 26$. From Fig. 10(d), a mode area of 824 $\mu m^2$ nearly independent of the duty cycle and bending orientation can be achieved. From all the results in Fig. 10, when $0.72 \leq \gamma \leq 0.73$, SM operation with a stable mode area can be achieved in the fiber bent in any orientation.

The effects of bending on the performance of the proposed fiber are shown in Fig. 11. From Fig. 11(a), the FM loss increases monotonically from higher than 0.5 dB/m to lower than 0.01 dB/m when $R_b$ increases from 13 cm to 20 cm. When $R_b \geq 15$ cm, the FM loss of the fiber bent in any orientation is always lower than 0.1 dB/m. From Fig. 11(b), the lowest HOM loss is always higher than 2.48 dB/m when the $R_b \leq 16$ cm. From Fig. 11(c), the HOMER is always greater than 10 no matter which orientation the fiber is bent in when $R_b \geq 13.5$ cm. Especially when 14 cm $\leq R_b \leq$ 15 cm, the HOMER is greater than 26. From Fig. 10(d), the mode area is independent of the bending orientation and increases monotonically from 789 $\mu m^2$ to 877 $\mu m^2$ when $R_b$ increases from 13 cm to 20 cm. From Fig. 11, when 15 cm $\leq R_b \leq 16$ cm, SM operation can be achieved in the fiber bent in any orientation. The corresponding smallest mode area is 824 $\mu m^2$.

The effects of operating wavelength on the performance of the proposed fiber are shown in Fig. 12. From Fig. 12(a), the FM loss of the fiber bent in any orientation is lower than 0.1 dB/m when 1.06 $\mu m \leq \lambda \leq 1.76$ $\mu m$. From Fig. 12(b), the lowest HOM loss is always higher than
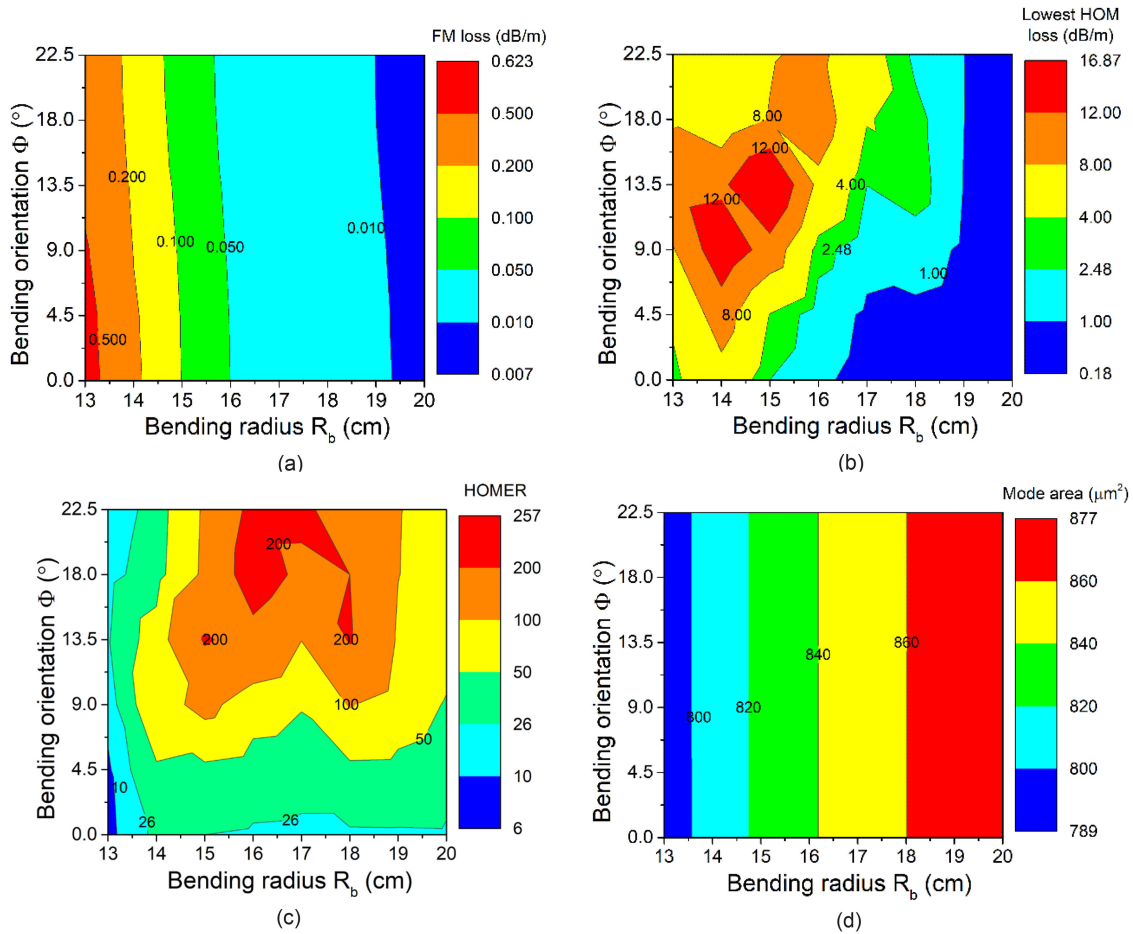
Fig. 11. Effects of bending on (a) the FM loss, (b) the lowest HOM loss, (c) the HOMER, and (d) the mode area of the proposed fiber when the bending orientation changes (The parameters are listed in Table 1 except $R_b$ and $\Phi$ are variables).

1.36 dB/m. Fig. 12(c) shows the HOMER is greater than 24 when 1 $\mu$m$\leq\lambda\leq$1.9 $\mu$m. The complicated dependences of the FM loss, the lowest HOM loss, and the HOMER on the wavelength are due to the loss variations of FM and the lowest-loss HOM induced by the resonant coupling which will not be discussed in detail in this paper. Fig. 12(d) shows the mode area increases monotonically from 794 $\mu$m$^2$ to 1144 $\mu$m$^2$ when $\lambda$ increases from 1.0 $\mu$m to 1.9 $\mu$m. From all the results in Fig. 12, SM operation can be achieved in a wide range of wavelengths from 1.06 $\mu$m to 1.76 $\mu$m no matter which orientation the fiber is bent in. A mode area of at least 824 $\mu$m$^2$ can be realized when the wavelength is in this range. This advantage of wideband single-mode operation in all bending orientations with a large mode area shows great potential in fiber lasers.

## 4. Fabrication Feasibility

The proposed SCF with a high-index ring in the core can be fabricated using the modified chemical vapor deposition (MCVD) process in conjunction with the rod-in-tube method and stack-and-draw technique. First, the core preform with a high-index ring can be realized by doping Yb$^{3+}$ and co-dopants ions to the inner wall of the silica glass tube during the MCVD process and then collapsing the deposited tube. Then, the preform consists of the core, index trench, and resonantring can be
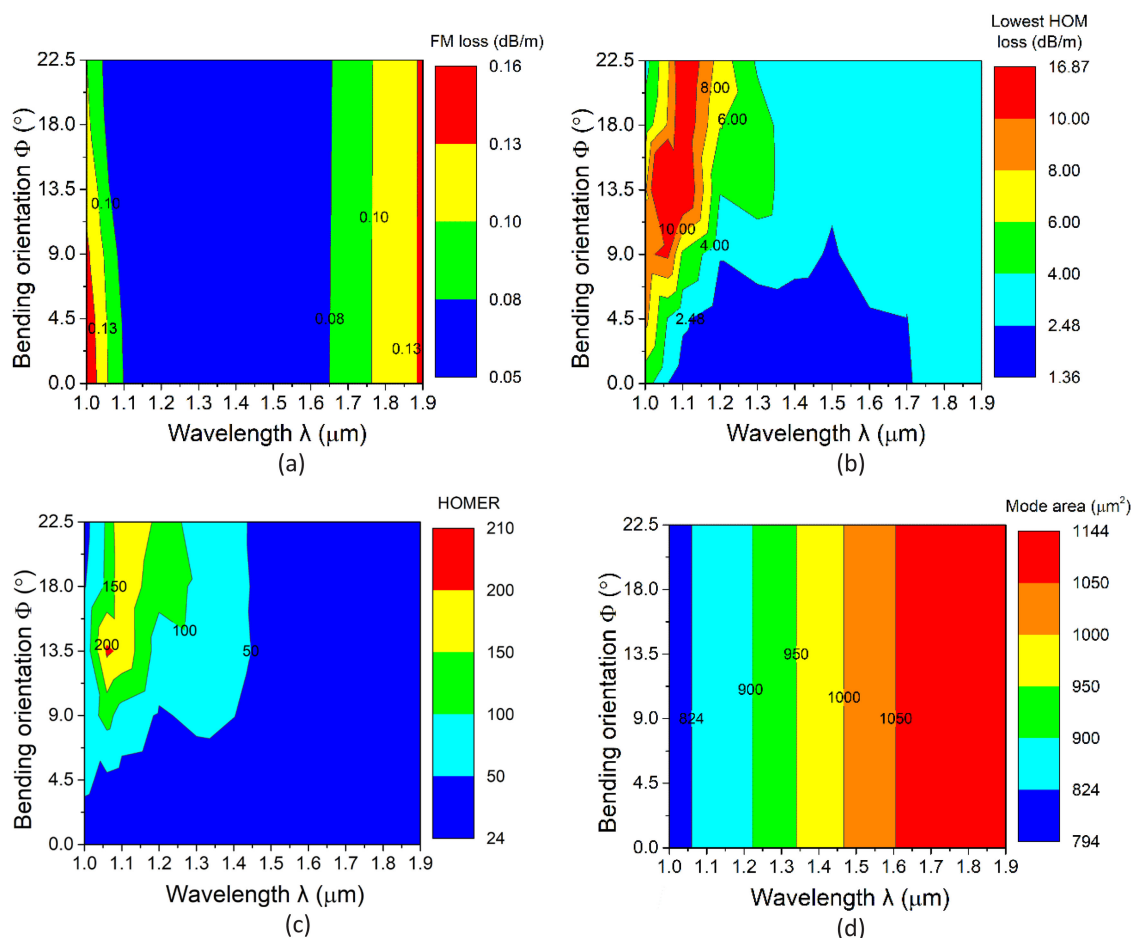
Fig. 12. Effects of operating wavelength on (a) the FM loss, (b) the lowest HOM loss, (c) the HOMER, and (d) the mode area of the proposed fiber when the bending orientation changes (The parameters are listed in Table 1 except λ and Φ are variables).

achieved by inserting the realized core rod into the glass tube with a fluorine-deposited inner wall. Finally, the fiber can be prepared using the stack-and-draw technique from the stacked preform with the realized preform surrounded by alternatively arranged F-doped, and index-raising dopants doped silica rods. It's important to mention a similar structure with two layers of high-index rings has been fabricated using the MCVD process in conjunction with the rod-in-tube method [40]. The silica-glass-based segmented cladding fiber has also been fabricated [41]. Therefore, the proposed fiber is possible to be manufactured with current-state-of-the-art fabrication technology.

## 5. Conclusion

A resonant-ring-assisted segmented cladding fiber with a high-index ring in the core is proposed. The improvement of the single-mode operation and the mode area enlargement brought by the high-index ring is demonstrated. The actual performance of the fiber under heat load is also displayed. The investigations of the effects of the high-index ring on the performance of the single-mode operation, the mode area, and the electric field distribution of FM of the proposed fiber show a well-designed high-index ring in the core can increase the difference of the leakage loss between the FM and HOMs and flatten the power distribution of the electric field. By taking these

advantages of the high-index-ring-assisted core, single-mode operation in all bending orientations is achieved and the mode area is enlarged. The further study on the effects of the duty cycle of cladding, bending, and operation wavelength on the fiber performance shows single-mode operation with a mode area larger than 824 $\mu$m$^2$ at a bending radius of 15 cm to 16 cm can be achieved when the operating wavelength ranges from 1.06 $\mu$m to 1.76 $\mu$m. This advantage of wideband single-mode operation in all bending orientations with a large mode area shows great potential in fiber lasers. The approach of adding a high-index structure in the core to improve single-mode operation and enlarge mode area shows great prospects in large mode area fibers.

## Acknowledgment

## References

[1] D. Richardson, J. Nilsson, and W. Clarkson, "High power fiber lasers: Current status and future perspectives," *J. Opt. Soc. Amer. B*, vol. 27, no. 11, pp. B63–B92, 2010.

[2] J. Nilsson, and D. N. Payne, "High-power fiber lasers," *Science*, vol. 332, no. 6032, pp. 921–922, 2011.

[3] C. Jauregui, J. Limpert, and A. Tünnermann, "High-power fibre lasers," *Nature Photon.*, vol. 7, no. 11, pp. 861–867, 2013.

[4] B. M. Kurade *et al.*, "Asymmetric-clad multi-trench fibers with large mode-area and controlled leakage loss," *Opt. Fiber Technol.*, vol. 48, pp. 235–241, 2019.

[5] D. Jain, Y. Jung, P. Barua, S. Alam, and J. K. Sahu, "Demonstration of ultra-low NA rare-earth doped step index fiber for applications in high power fiber lasers," *Opt. Exp.*, vol. 23, no. 6, pp. 7407–7415, 2015.

[6] J. Sun, Z. Kang, J. Wang, *et al.*, "Novel bending-resistant design of two-layer low-index trench fiber with parabolic-profile core," *Opt. Express*, vol. 22, no. 15, pp. 18036–43, 2014.

[7] M. N. Zervas, and C. A. Codemard, "High power fiber lasers: A review," *IEEE J. Sel. Topics Quant. Electron.*, vol. 20, no. 5, pp. 219–241, Sep./Oct. 2014.

[8] D. Jain, J. Sahu, and S. Fleming, "Breaking the stringent trade-off between mode area and NA for efficient high-power fiber lasers around 2 $\mu$m," *J. Lightw. Technol.*, vol. 99, pp. 1–1, 2020.

[9] L. Kong *et al.*, "Thermally induced mode loss evolution in the coiled ytterbium doped large mode area fiber," *Opt. Exp.*, vol. 25, no. 19, pp. 23437–23450, 2017.

[10] A. V. Smith, and J. J. Smith, "Mode instability in high power fiber amplifiers," *Opt. Exp.*, vol. 19, pp. no. 11, pp. 10180–10192, 2011.

[11] F. Stutzki *et al.*, "High-speed modal decomposition of mode instabilities in high-power fiber lasers," *Opt. Lett.*, vol. 36, no. 23, pp. 4572–4574, 2011.

[12] S. Yoo *et al.*, "Photodarkening in Yb-doped aluminosilicate fibers induced by 488 nm irradiation," *Opt. Lett.*, vol. 32, no. 11, pp. 1626–1628, 2008.

[13] J. Li *et al.*, "Thermal bleaching of photodarkening and heat-induced loss and spectral broadening in Tm3+-doped fiber," *Opt. Exp.*, vol. 28, no. 15, pp. 21845–21853, 2020.

[14] D. Jain *et al.*, "Highly efficient Yb-free er-la-al doped ultra-low NA large mode area single-trench fiber laser," *Opt. Exp.*, vol. 23, no. 22, pp. 28282–28287, 2015.

[15] J. Limpert, *et al.* "Yb-doped large-pitch fibers: Effective single-mode operation based on higher-order mode delocalization," *Light: Sci. App.*, vol. 1, pp. 1–5, 2012.

[16] J. C. Knight, "Photonic crystal fibers and fiber lasers," *J. Opt. Soc. Amer. B*, vol. 24, no. 8, pp. 1661–1668, 2007.

[17] L. Dong *et al.*, "Ytterbium-doped all glass leakage channel fibers with highly fluorine-doped silica pump cladding," *Opt. Exp.*, vol. 17, no. 11, pp. 8962–8969, 2009.

[18] F. Kong *et al.*, "Flat-top mode from a 50 $\mu$m-core Yb-doped leakage channel fiber," *Opt. Exp.*, vol. 21, no. 26, pp. 32371–32376, 2013.

[19] Y. A. Uspenskii *et al.*, "Effect of polymer coating on leakage losses in bragg fibers," *Opt. Lett.*, vol. 32, no. 10, pp. 1202–1204, 2007.

[20] K. Fanting *et al.*, "Polarizing ytterbium-doped all-solid photonic bandgap fiber with ∼1150 $\mu$m(2) effective mode area," *Opt. Exp.*, vol. 23, no. 4, pp. 4307–4312, 2015.

[21] X. Ma, Z. Cheng, I. N. Hu, *et al.*, "Single-mode chirally-coupled-core fibers with larger than 50m diameter cores," *Opt. Express*, vol. 22, no. 8, pp. 9206–9219, 2014.

[22] A. Siegman, "Gain-guided, index-antiguided fiber lasers," *J. Opt. Soc. Amer. B*, vol. 24, pp. 1677–1682, 2007.

[23] S. Ma *et al.*, "Design and analysis of a modified segmented cladding fiber with parabolic-profile core," *Laser Phys. Lett.*, vol. 15, no. 3, pp. 035104-035110, 2018.

[24] D. Jain *et al.*, "Extending single mode performance of all-solid large-mode-area single trench fiber," *Opt. Exp.*, vol. 22, no. 25, pp. 31078–31091, 2014.

[25] D. Jain, C. Baskiotis, and J. K. Sahu, "Mode area scaling with multi-trench rod-type fibers," *Opt. Exp.*, vol. 21, no. 2, pp. 1448–1455, 2013.

[26] D. Jain, C. Baskiotis, and J. K. Sahu, "Bending performance of large mode area multi-trench fibers," *Opt. Exp.*, vol. 21, no. 22, pp. 26663–26670, 2013.

[27] V. Rastogi, and K. S. Chiang, "Propagation characteristics of a segmented cladding fiber," *Opt. Lett.*, vol. 26, no. 8, pp. 491–493, 2001.

[28] A. Millo, I. Naeh, and A. Katzir, "Single-mode segmented cladding fibers for the middle infrared," *J. Lightw. Technol.*, vol. 25, no. 8, pp. 2115–2121, 2007.

[29] S. Ma *et al.*, "Detailed study of bending effects in large mode area segmented cladding fibers," *Appl. Opt.*, vol. 55, no. 35, pp. 9954–9960, 2016.

[30] S. Ma *et al.*, "Bending-resistant design of a large mode area segmented cladding fiber with resonant ring," *J. Lightw. Technol.*, vol. 36, no. 14, pp. 2844–2849, 2018.

[31] S. S. Aleshkina *et al.*, "High-order mode suppression in double-clad optical fibers by adding absorbing inclusions," *Sci. Reports*, vol. 10, no. 1, pp.7174–7185, 2020.

[32] D. Marcuse, "Influence of curvature on the losses of doubly clad fibers," *Appl. Opt.*, vol. 21, no. 23, pp. 4208–4213. 1982.

[33] K. Nagano, S. Kawakami, and S. Nishida, "Change of the refractive index in an optical fiber due to external forces," *Appl. Opt.*, vol. 17, no. 13, pp. 2080–2085, 1978.

[34] L. Dong, X. Peng, and J. Li, "Leakage channel optical fibers with large effective area," *J. Opt. Soc. Amer. B.* vol. 24, no. 8, pp. 1689–1697, 2007.

[35] X. Wang, S. Lou, and W. Lu, "Bending orientation insensitive large mode area photonic crystal fiber with triangular core," *IEEE Photon. J.*, vol. 5, no. 4, Aug. 2013, Art. no. 7100408.

[36] F. Poletti, "Nested antiresonant nodeless hollow core fiber," *Opt. Exp.*, vol. 22, no. 20, pp. 23807–23828, 2014.

[37] M. S. Habib, J. E. Antonio-Lopez, C. Markos, A. Schülzgen, and R. Amezcua-Correa, "Single-mode, low loss hollow-core anti-resonant fiber designs," *Opt. Exp.*, vol. 27, no. 4, pp. 3824–3836, 2019.

[38] M. David C. Brown, and H. J. Hoffman, "Thermal, stress, and thermo-optic effects in high average power double-clad silica fiber lasers," *IEEE J. Sel. Topics Quant. Electron.*, vol. 37, pp. 207–217, Feb. 2001.

[39] E. Coscelli, R. Dauliat, F. Poli, D. Darwich, A. Cucinotta, S. Selleri *et al.*, "Analysis of the modal content into large-mode-area photonic crystal fibers under heat load," *IEEE J. Sel. Topics Quant. Electron.*, vol. 22, pp. 323–330, Mar. 2016.

[40] S. S. Aleshkina *et al.*, "High-peak-power femtosecond pulse generation by nonlinear compression in a Yb-doped hybrid fiber," *IEEE Photon. J.*, vol. 11, no. 5, Oct. 2019, Art. no. 7103411.

[41] B. Hooda *et al.*, "Segmented cladding fiber fabricated in silica-based glass," *Opt. Eng.*, vol. 54, no. 7, 2015, Art. no. 075103.